An Electron Spin Resonance and Electron Spin-Echo Modulation Study of Paramagnetic Rh Species Generated in Ca-Y and Na-Y Zeolites

Daniella Goldfarb and Larry Kevan*

Contribution from the Department of Chemistry, University of Houston, Houston, Texas 77004.
Received September 15, 1986

Abstract: Paramagnetic Rh species generated in RhNa-Y and RhCa-Y zeolites after various treatments were characterized by using electron spin resonance (ESR) and electron spin-echo modulation (ESEM) spectroscopies. Activation in flowing oxygen at 500 °C β-hydrogen a considerable amount of Rh(II) located in site I in the hexagonal prism of the zeolite structure for 3 wt % Rh in RhNa-Y zeolite. Samples of 1 wt % Rh in RhNa-Y and RhCa-Y did not show any paramagnetic signals. Adsorption of various adsorbates such as water, ammonia, methanol, carbon monoxide, and oxygen on activated samples induced a considerable increase in the ESR intensities. Adsorption of oxygen and carbon monoxide yields the corresponding adducts which are located in the α-cage of the zeolite structure. Hydration generated a species which is coordinated to three water molecules. Adsorption of methanol on RhNa-Y generated a species H2 which is also formed after reduction of RhNa-Y with H_2, suggesting that the methanol molecule undergoes a reaction to generate products which further reduce Rh(III) species in the β-cage of the zeolite structure to Rh(II). No significant differences were observed between RhNa-Y and RhCa-Y except for the formation of different Rh(II) species after methanol adsorption in RhCa-Y and the generation of a larger amount of Rh(II) in site I in RhNa-Y. These results are compared to previously obtained data in RhNa-X and RhCa-X to account for the effect of the cocations and the Si/Al ratio on the generation of Rh(II) species in zeolites.

In previous publications[1-3] we have reported on the formation of Rh(II) species in Na-X and Ca-X zeolites following various activation, adsorption, oxidation, and reduction processes. We found that exchange of Na^+ cocations with Ca^{2+} cocations in X zeolite had a considerable effect on the nature of the Rh(II) species formed in terms of both location within the zeolite structure and interaction with adsorbates. In the present study we present results obtained from similar experiments performed on Rh-exchanged Ca-Y sequence involving Na-Y zeolites. X and Y zeolites are structurally identical, but they differ in the Si/Al ratio, 1.4 and 2.5, respectively. Accordingly, Y zeolite contains fewer charge balancing cocations. Comparison of these results with those obtained from Ca-X and Na-X provides a better understanding of the factors controlling the generation and location of paramagnetic Rh species in X and Y zeolites.

Paramagnetic Rh species in Na-Y have been reported previously;[4-6] however, the experimental results are not in agreement probably due to differences in the activation and exchange procedures. On the basis of hyperfine β-hydrogen due to the ^{103}Rh nuclei Atanasova et al.[5] reported the formation of Rh(I)-Rh(0) or Rh(II)-Rh(I) ion pairs after heating under vacuum to 500 °C and oxidation with O_2 at 500 °C, whereas Naccache et al.[4] reported the formation of Rh(II) monomers after heating the sample to 500 °C in flowing oxygen and then evacuating. In addition to new experiments performed in RhNa-Y, we have repeated some of the previously reported experiments[5,6] in order to obtain a more consistent comparison with our RhCa-X, RhCa-Y, and RhNa-X results.

Experimental Section

The zeolite Y used was Linde YZ-52 (Na-Y). Ca-Y was obtained by exchange with 0.2 M calcium chloride solution five times at 343 K to obtain fully exchanged Ca-Y. Rh cations were exchanged into both Ca-Y and Na-Y with $[Rh(NH_3)_5Cl]Cl_5$ (Strem Chemical, Inc.). The exchange was carried out at room temperature by dropwise addition of 25 mL of 4 and 12 mM solutions of $[Rh(NH_3)_5Cl]Cl_2$ in triply distilled water to a Ca-Y or Na-Y slurry of 0.5 g in 450 mL of water. The mixture was stirred for 24 h, filtered, and dried at room temperature. The samples contained 1 and 3 wt % Rh as measured by commercial atomic absorption analysis. This Rh loading corresponds to ~2 and ~6 Rh cations per unit cell. The samples were activated in flowing oxygen up to various temperatures as described previously.[1] Reduction and oxidations were performed with H_2 and O_2 as described.[2] All adsorptions were carried out at room temperature, and the samples were sealed at 77 K in 3 mm o.d. by 2 mm i.d. Suprasil quartz ESR tubes.

ESR spectra were recorded at 77 K and at room temperature with a modified Varian E-4 spectrometer interfaced with a Tracor signal averager. Electron spin echo modulation (ESEM) spectra were recorded at 4.2 K with a home-built spectrometer described elsewhere[7] interfaced with a Nicolet 1280 computer. The pulse sequence for field swept ESE was $(2\pi/3)_x$-τ-$(2\pi/3)_x$-τ-echo, where τ is held constant while the magnetic field is scanned. ESEM spectra were obtained with the following sequence: $\pi/2$-τ-$\pi/2$-T-$\pi/2$-τ-echo with the following phase cycling $(x,x,x) + (-x,-x,x) - (-x,-x,-x) - (x,x,-x)$ to eliminate the two-pulse gliches[8,9] and base line drift. The modulation is observed by recording the stimulated echo amplitude as a function of T while τ is selected between 0.27 and 0.30 μs to suppress ^{27}Al modulation.[10] Due to the Nicolet pulse programmer's limitation, delays shorter than 0.16 μs cannot be obtained; accordingly our ESEM traces start from $T = 0.16$ μs.

Theory and Analysis

The theory of ESEM has been described in detail.[10-13] For deuterium modulation ($I = 1$), neglecting the quadrupole interaction the normalized three-pulse echo modulation is given by

$$V(\tau,T) = 1 - 8k\{\sin^2(\omega_\alpha\tau/2)\sin^2[\omega_\beta(\tau+T)/2] + \sin^2[\omega_\alpha(\tau+T)/2]\sin^2(\omega_\beta\tau/2)\}/3 + 8k^2\{\sin^4(\omega_\alpha\tau/2)\sin^4[\omega_\beta(\tau+T)/2] + \sin^4[\omega_\alpha(\tau+T)/2]\sin^4(\omega_\beta\tau/2)\}/3$$

where τ and T are the separations between the first and second and the second and third pulses respectively and $k = (\omega_1 B/\omega_\alpha\omega_\beta)^2$,

(1) Goldfarb, D.; Kevan, L. *J. Phys. Chem.* **1986**, *90*, 264. (r) Periana, R. A.; Bergman, R. G. *J. Am. Chem. Soc.* **1986**, *108*, 7332 and references cited therein.
(2) Goldfarb, D.; Kevan, L. *J. Phys. Chem.* **1986**, *90*, 2137.
(3) Goldfarb, D.; Kevan, L. *J. Phys. Chem.* **1986**, *90*, 5787.
(4) Naccache, C.; Ben-Taarit, Y.; Boudart, M. In *Molecular Sieves II*; Katzer, J. R., Ed.; American Chemical Society: Washington, D.C., 1977; ACS Symp. Ser. 40, p 15. (n) Cassady, C. J.; Freiser, B. S. *J. Am. Chem. Soc.* **1985**, *107*, 1573.
(5) Atanasova, V. D.; Shvets, V. A.; Kazanskii, V. B. *Kinet. Catal.* **1979**, *18*, 828.
(6) Narayana, M.; Kevan, L.; Naccache, C. *J. Catal.* **1984**, *86*, 413.
(7) Ichikawa, T.; Kevan, L.; Narayana, P. A. *J. Phys. Chem.* **1979**, *86*, 3378.
(8) Bowman, M. K.; a footnote: Mims, W. B. *J. Magn. Reson.* **1984**, *59*, 293.
(9) Fauth, J. M.; Schweiger, A.; Braunschweiler, L.; Forrer, J.; Ernst, R. R. *J. Magn. Reson.* **1986**, *66*, 74.
(10) Kevan, L. In *Time Domain Electron Spin Resonance*; Kevan, L.; Schwartz, R. N., Eds.; Wiley-Interscience: New York, 1979; Chapter 8.
(11) Mims, W. B. *Phys. Rev. B* **1972**, *5*, 2409; *6*, 3543.
(12) Mims, W. B.; Peisach, J.; Davis, J. L. *J. Chem. Phys.* **1972**, *76*, 2860; **1977**, *66*, 5536.
(13) Dikanov, S.; Shubin, A. A.; Parmon, U. N. *J. Magn. Reson.* **1981**, *42*, 4748.

0002-7863/87/1509-2303$01.50/0

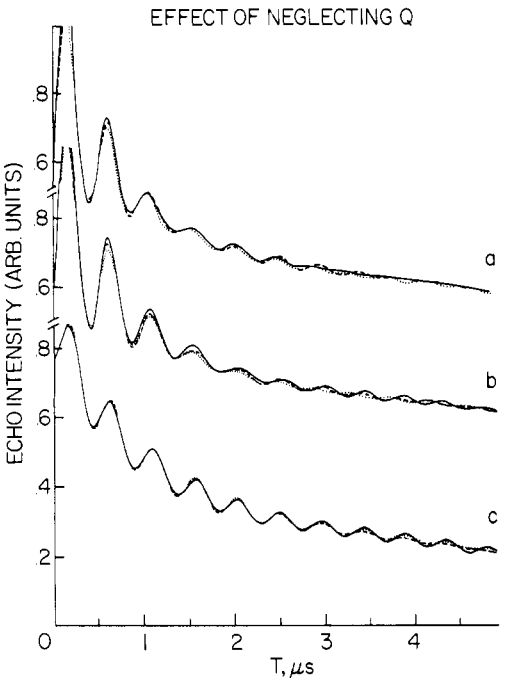

Figure 1. (a) Calculated ESEM using exact solution including quadrupole interaction tensor multiplied by a decay function. The parameters used were A = 0.15 MHz, R = 0.3 nm, N = 4, Q = 0.2 MHz, ψ = 50°; best fit obtained using ratio analysis neglecting the quadrupole interaction with A = 0.15 MHz, R = 0.31 nm, and N = 4 (---); fit with A = 0.1 MHz, R = 0.3 nm and N = 3 (···). (b) Same as in case a but with ψ = 0° (—); best fit obtained with A = 0.1 MHz, R = 0.31 nm, N = 4, and Q = 0.0 MHz (---); fit with A = 0.05 MHz, R = 0.3 nm, N = 3 and Q = 0.0 MHz (···). (c) Wame as case b with A = 0.0 MHz, R = 0.4 nm, N = 6, and Q = 0.2 MHz (—); fit obtained with A = 0.0 MHz, R = 0.4 nm, N = 6, and Q = 0.0 MHz (---); fit with A = 0.05 MHz, R = 0.43 nm, N = 9, and Q = 0.0 MHz (···). All results were calculated with H_0 = 3820 G and τ = 0.28 μs.

$\omega_\alpha = [(A/2 + \omega_I)^2 + (B/2)^2]^{1/2}$, $\omega_\beta = [(A/2 - \omega_I)^2 + (B/2)^2]^{1/2}$, $A = T_\perp(3\cos^2\theta - 1) + 2\pi A$, $B = 3T_\perp \sin\theta\cos\theta$, and $T_\perp = gg_n\beta\beta_n/\hbar r^3$. ω_I is the deuterium Larmor frequency at the magnetic field H_0, A is the isotropic hyperfine constant, θ is the angle between H_0 and the vector joining the electron and the nuclei, and R is the electron–nuclei distance.

For a disordered system such as the zeolites under study the total modulation is obtained by averaging over all orientations θ. Since the geometry of the Rh species formed in zeolites is unknown, we analyzed the data using the spherical model,[10] in which the angular integration of the anisotropic quantities is performed neglecting mutual nuclear arrangement and the **g** tensor is considered as isotropic. In this case the modulation from N equivalent nuclei is given according to

$$V(\tau,T) = \left[\frac{1}{4\Pi}\int_0^{2\Pi}\int_0^{\Pi} V(\tau,T,\theta)\sin\theta\,d\theta\,d\phi\right]^N$$

The best fit parameters, N, R, and A, are obtained by using the ratio analysis described in ref 13. The spherical model in most cases is a good approximation, especially for distances >0.4 nm and where the number of interacting nuclei is fairly large. In the case of Rh interaction with adsorbates within the zeolite cages, a refinement of the geometry obtained by the spherical model using a correlated structure for shorter distances, as suggested by Iwasaki and Toriyama,[14] is impractical since many different coordination geometries can be used due to the fact that the number of framework oxygens is only deduced indirectly and most often is not certain.

The effect of the quadrupole interaction tensor on the ESEM has been discussed in several publications.[15-21] Including the quadrupole interaction in the calculation is extremely time consuming especially when the hyperfine and quadrupole tensors are not colinear which is always the case in deuteriated adsorbates where the principal axis of the quadrupole tensor is along the C–D or O–D bond, and the principal axis of the hyperfine tensor is along the Rh—D vector.

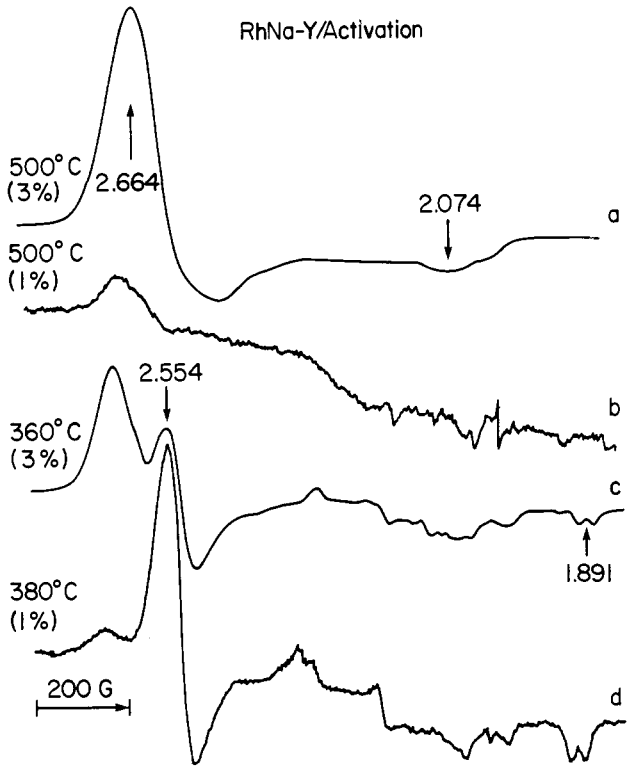

Figure 2. ESR spectra of RhNa–Y, 1 wt % and 3 wt %, recorded at 77 K as a function of activation temperature. The gains are 2 × 10^2, 5 × 10^3, 5 × 10^2, and 4 × 10^3, respectively.

In order to assess the error introduced by neglecting the quadrupole interaction for deuterium, we investigated the following. We calculated the ESEM for three different cases where the axially symmetric quadrupole tensor, not necessarily coinciding with the dipolar tensor, was taken into account by use of exact diagonalization. The angle between the principal axes of the two tensors is Ψ. These ESEM traces were multiplied by a decay function to resemble experimental data. Then, we treated these traces as experimental data and simulated them using ratio analysis, neglecting the quadrupole tensor, to obtain the best fit parameters A, R, and N. The results are shown in Figure 1. All three cases show that at shorter times up to ~2 μs the fit is rather good; the disagreement usually occurs at longer times. Neglecting the quadrupole tensor does not seem to affect the deduced distance of interaction R to a great extent; however, it does seem to introduce some ambiguity in the number of the interacting nuclei, i.e., 3 or 4 in case a and 6 or 9 in case c. It also introduces ~0.05 MHz uncertainty in A.

Results

Activation. Activation at 400–500 °C produces similar ESR spectra for both RhCa–Y and RhNa–Y (Figures 2 and 3).

(14) Ichikawa, T.; Kevan, L.; Bowman, M. K.; Dikanov, S. A.; Tsvetkov, Y. D. *J. Chem. Phys.* **1979**, *71*, 1167.
(15) Iwasaki, M.; Toriyama, K. *J. Chem. Phys.* **1985**, *82*, 5415.
(16) Shubin, A. A.; Dikanov, S. A. *J. Magn. Reson.* **1983**, *52*, 1.
(17) Romanelli, M.; Narayana, M.; Kevan, L. *J. Chem. Phys.* **1984**, *80*, 4044.
(18) Heming, M.; Narayana, M.; Kevan, L. *J. Chem. Phys.* **1985**, *83*, 1478.
(19) Romanelli, M.; Narayana, M.; Kevan, L. *J. Chem. Phys.* **1985**, *83*, 4395.
(20) Shubin, A. A.; Dikanov, S. A. *J. Magn. Reson.* **1985**, *64*, 185.
(21) Ichikawa, T. *J. Chem. Phys.* **1985**, *83*, 3790.
(22) Ben Taarit, Y.; Vedrine, J. C.; Dutel, J. K.; Naccache, C. *J. Magn. Reson.* **1978**, *31*, 251.

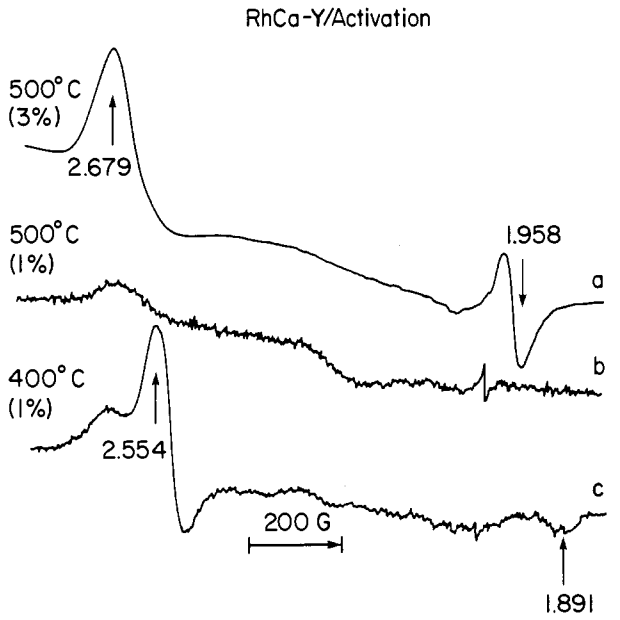

Figure 3. ESR spectra of RhCa-Y, 3 wt % and 1 wt %, recorded at 77 K as a function of activation temperature. The gains are 8×10^2, 5×10^3, and 4×10^3, respectively.

Activation of 1 wt % RhCa-Y and RhNa-Y at 380–400 °C generates a major species with $g_\perp = 2.554$ and $g_\parallel = 1.981$ with the $g_\parallel$ line split (30 G) due to interaction with the Rh nuclei ($I = {}^1/_2$). This species, termed species A, is shown in Figure 2d and is not observed at room temperature. When a sample of 3 wt % RhNa-Y is activated at 400–500 °C species C is formed (Figure 2a); however, at an activation temperature of 360 °C (Figure 2c), species A appears with species C ($g_\perp = 2.664$, $g_\parallel = 2.074$). These values are close to the values obtained by Naccache et al.[4] We see no evidence for Rh^+–Rh^0 or Rh^{2+}–Rh^+ ion pairs as described by Atanasova et al.[3] Activation of 3 wt % RhCa-Y at 500 °C yields an additional species at $g_\parallel = 1.958$. Species C is observed at room temperature as well. Activation of 1 wt % RhCa-Y and RhNa-Y at 500 °C generates practically no paramagnetic species (Figures 2b and 3b); it seems that a higher degree of exchange facilitates the formation of species C.

As explained previously,[1] we assign the ESR signals formed after activation to Rh(II). Species A appeared in RhCa-X as well, although in smaller amounts, and in the $g_\parallel$ feature the hyperfine splitting was not resolved. In RhNa-X species A is also formed after activation to 400 °C;[1] however, the $g_\perp$ feature is split due to nonaxiality of the tensor with $g_{xx} = 2.516$, $g_{yy} = 2.560$, $g_{zz} = 1.883$. These values are very close to those observed in RhCa-X, RhCa-Y, and RhNa-Y. The relation $g_\perp > g_e > g_\parallel$ for a low spin d^7 cation occurs when the ground state is d_{xy}. A rather large elongated tetragonal distortion would result in a d_{xy} ground state.[22]

Species C is also generated in RhNa-X after activation to 500 °C. At higher Rh loading one can observe species C at lower activation temperatures of 400–450 °C.[1] The axial **g** tensor with $g_\perp > g_\parallel \sim g_e$ is indicative of the unpaired electron residing in the Rh $d_{z^2-r^2}$ orbital which occurs in tetragonally elongated octahedral symmetry.[2]

The response of RhNa-Y to reduction with H_2 depends on the Rh loading. In a 3 wt % sample, species A is readily reduced with 240 Torr of H_2 at room temperature as seen in Figure 4a, whereas after exposing 1 wt % RhNa-Y activated to the same temperature (400 °C) to 140 Torr of H_2 at room temperature signal A did not disappear. Signal A in 1 wt % RhCa-Y did not disappear as well under the same conditions. Note that in 3 wt % RhNa-Y signal C was not affected by H_2 at room temperature; however, heating the sample in H_2 to 200 °C resulted in a decrease in the amount of species C and the appearance of a new species at $\mathbf{g} \sim 2.154$ (Figure 4b). This same species is obtained after reducing 1 wt % RhCa-Y (Figure 4c).

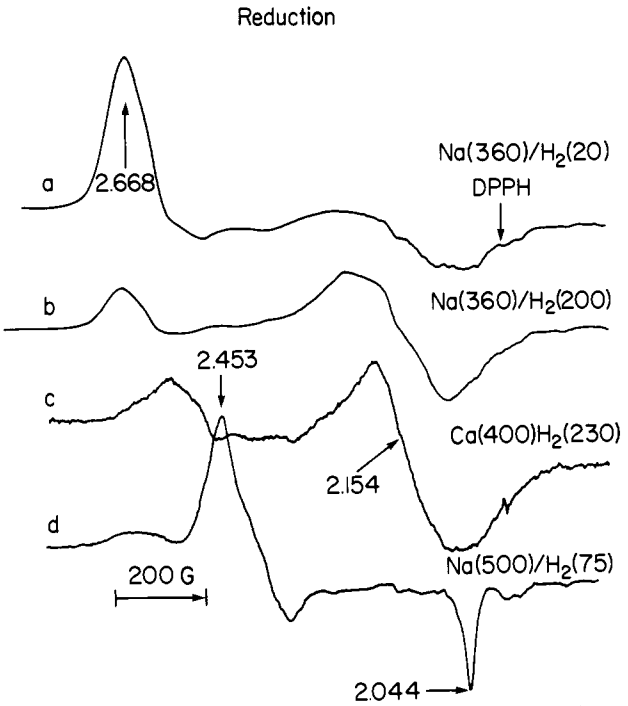

Figure 4. ESR spectra recorded at 77 K of (a) 3 wt % RhNa-Y activated at 360 °C and reduced with 240 Torr of H_2 at room temperature, (b) same heated at 200 °C for 1.5 h, (c) 1 wt % RhCa-Y activated at 400 °C and reduced with 200 Torr of H_2 at 230 °C, and (d) 1 wt % RhNa-Y activated at 500 °C after reduction with 140 Torr of H_2 at 75 °C. The gains are 6.3×10^2, 5×10^2, 2.5×10^3, and 2×10^3, respectively.

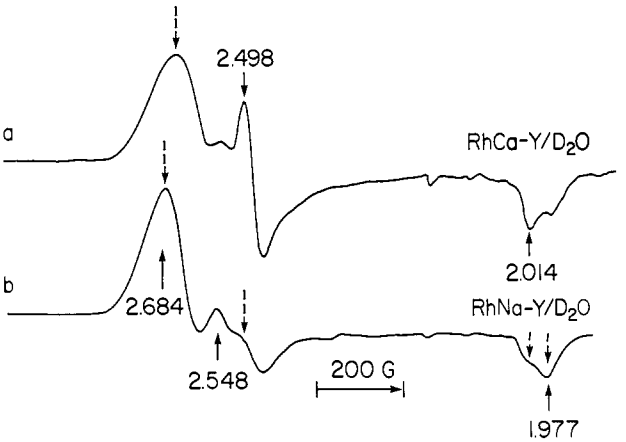

Figure 5. ESR spectra recorded at 77 K of (a) 1 wt % RhCa-Y activated at 500 °C and completely rehydrated with D_2O and (b) 1 wt % RhNa-Y treated similarly. The gains are 6.3×10^2 and 2×10^2, respectively. The dashed arrows indicate the positions at which ESE experiments were performed.

Reduction of RhNa-X under the same conditions[2] gave different species. RhNa-X (1–2 wt %) activated to 400 °C generated after H_2 reduction at 200 °C species H1 with an isotropic **g** tensor ($\mathbf{g} = 2.165$) which showed a dynamic Jahn–Teller effect. Furthermore, species A did not disappear at room temperature but did when reduction was performed at 200 °C. Reduction of samples activated to 500 °C generated a different species with $g_\perp = 2.44$ and $g_\parallel = 2.03$. This species is observed in RhNa-Y under similar conditions (Figure 4d). Reduction of RhCa-X generated the same ESR spectrum as in RhCa-Y and RhNa-Y.[3]

Hydration. Hydration of 1 wt % RhCa-Y and RhNa-Y activated in the 400–500 °C range generated similar species differing only in their relative amounts. In both cases water adsorption was accompanied by a considerable increase in spin concentration (Figure 5). This increase in total spin concentration has been

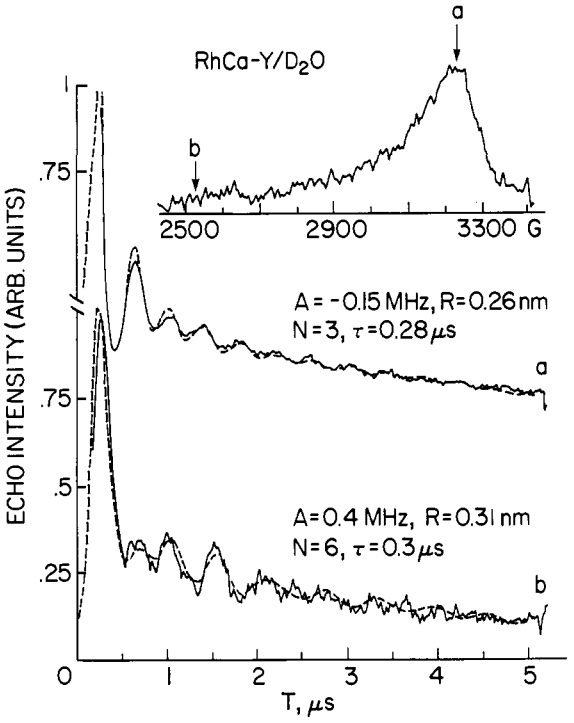

Figure 6. Field swept ESE of 1 wt % RhCa–Y activated at 500 °C after D_2O adsorption recorded with τ = 0.29 μs at the top and the three-pulse ESEM recorded at field positions a and b. The solid lines represent the experimental spectra whereas the dashed lines are the calculated ESEM. The parameters used for the calculations are indicated on the figure.

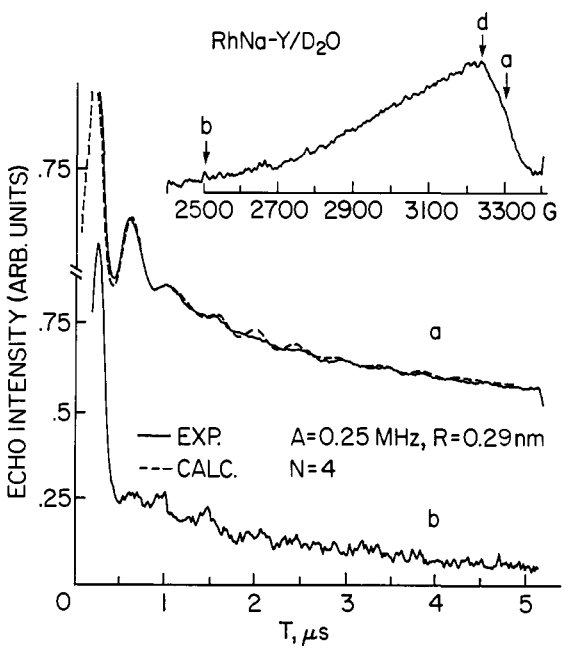

Figure 7. Field swept ESE of 1 wt % RhNa–Y activated to 500 °C after D_2O adsorption recorded with τ = 0.35 μs at the top and the three-pulse ESEM recorded at field positions a and b. ESEM at position a was obtained with τ = 0.28 μs and the simulation parameters are listed on the figure. Trace b was recorded with τ = 0.31 μs.

observed in both RhNa–X[1] and RhCa–X[3] and it was attributed to dissociation of Rh(II) diamagnetic dimers. Partial hydration of 1 wt % RhNa–Y generated a major species with $g_\perp$ = 2.684 and $g_\parallel$ = 2.004 and another species with a much smaller relative concentration with $g_\perp \sim 2.00$. Further hydration to saturation generated additional species with $g_\perp$ = 2.548 and 2.498. As in RhNa–X[1] the hydration occurs in two steps, first species C is formed and then additional species bound to water appear. The ESR spectrum of fully hydrated 1 wt % RhCa–Y is similar to the RhNa–Y spectrum except that the line at 2.498 is more intense. Exposure of the RhCa–Y sample to 100 Torr of O_2 for 24 h caused a reduction in the intensity of the 2.498 and 2.014 lines from which we deduced that they correspond to the same species. Nevertheless, inspection of the relative intensities of the lines at the **g** = 2 region in a number of different samples suggests that additional species are contributing to the signal in this region.

Field swept ESE spectra of corresponding RhCa–Y and RhNa–Y samples (Figures 6 and 7) show a strong signal at $H \cong 3250$ G which corresponds to $\mathbf{g} \sim 2$ and a much weaker signal at H = 2500 G ($\mathbf{g} \sim 2.6$). The differences between the ESR spectra and the field swept ESE spectra could arise from (a) differences in the phase memory time of the species present and (b) dependence on τ for strongly modulated spectra.

In general the echo intensity observed in Rh-exchanged Y zeolite is weaker than in X zeolite due to paramagnetic impurities such as Fe^{3+} and Mn^{2+}. The signal of Mn^{2+} ($I = {}^5/_2$) is a relatively weak isotropic six-line spectrum with a separation of ~84 G at $\mathbf{g} \cong 2.00$ which can be seen in most samples. Figure 6 shows the ESEM recorded from RhCa–Y at positions a and b, H = 3221 and 2515 G, respectively. The excited lines are also indicated by arrows in Figure 5. The bottom trace, which corresponds to species I, corresponds to Rh interacting with 6 deuteriums (3 water molecules) at a distance of 0.31 nm. The trace recorded at H = 3221 G could not be simulated very welll, probably due to overlapping of species; nevertheless it is indicative of the proximity between the Rh cation and the deuterium of water or hydroxyl groups. The results obtained for species I are in good agreement with results obtained from RhCa–X[3], where the ESEM spectra were simulated by using N = 6, R = 0.3 nm, and A = 0.4 MHz.

The ESR spectrum of hydrated RhCa–X[3] is similar to that of hydrated RhCa–Y except for the species **g** = 2.548 which does not appear in hydrated RhCa–X. The ESEM results obtained from 1 wt % RhNa–Y are shown in Figure 7. The bottom trace looks very much like the corresponding trace in RhCa–Y, it shows very deep modulation with the echo decaying rapidly. We did not attempt to simulate this ESEM due to lack of details. ESEM recorded at positions a and d gave identical patterns. The simulation indicates a short interaction distance (Figure 7a) with directly coordinated water molecules or hydroxyl groups.

While the ESR spectra obtained from hydrated RhNa–X and RhCa–X and hydrated RhCa–Y and RhNa–Y are quite similar, the ESEM indicates major differences. The major species in RhNa–X (species C) is not directly coordinated to water[1] while in Rh-exchanged Na–Y, Ca–Y, and Ca–X the major species, I, is directly coordinated to three water molecules.

Interaction with Methanol and Ammonia. Methanol adsorption on 1 wt % RhNa–Y and RhCa–Y is followed by an increase in the spin concentration. The ESR spectrum of 1 wt % RhNa–Y after methanol adsorption reveals the existence of several species (Figure 8a), in contrast to the single species C formed in RhNa–X.[1] The line at **g** = 2.648 could correspond to either species C or species I. Unfortunately this sample gave a rather poor echo and ESEM were recorded for CD_3OH and CH_3OD only at H = 2730 G (position shown by the arrow in Figure 8a). No modulation was observed in either case. Upon evacuation at room temperature the line at **g** = 2.044 disappeared. All signals besides those at **g** = 2.044 and **g** = 2.035 could be observed at room temperature. A similar spectrum was observed for a RhNa–Y sample activated at 380 °C, although the intensity of the lines in the **g** = 2 region was larger.

Note that the spectrum after methanol adsorption is quite similar to that observed after reduction of a RhNa–Y sample activated at 500 °C (Figure 4d), and the species with $g_\perp$ = 2.453 and $g_\parallel$ = 2.044 in both spectra indicate that methanol is involved in a reaction which subsequently generates Rh(II). The lack of deuterium modulation indicates that this species is not coordinated to methanol and supports the above suggestion. In RhCa–Y fewer species are formed after methanol adsorption (Figure 8b,c) and the total spin concentration is smaller. The RhCa–Y spectrum is quite similar to that observed in RhCa–X under the same conditions. Note that there are some differences between the

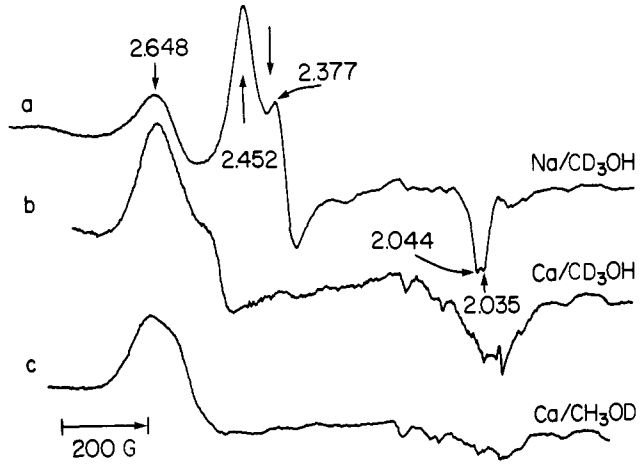

Figure 8. ESR spectra at 77 K of (a) 1 wt % RhNa-Y activated at 460 °C after CD_3OH adsorption, (b) 1 wt % RhCa-Y activated at 400 °C after CD_3OH adsorption, and (c) same as case b after activation at 500 °C and CH_3OD adsorption. The gains are 2×10^3, 2×10^3, and 1.6×10^3, respectively.

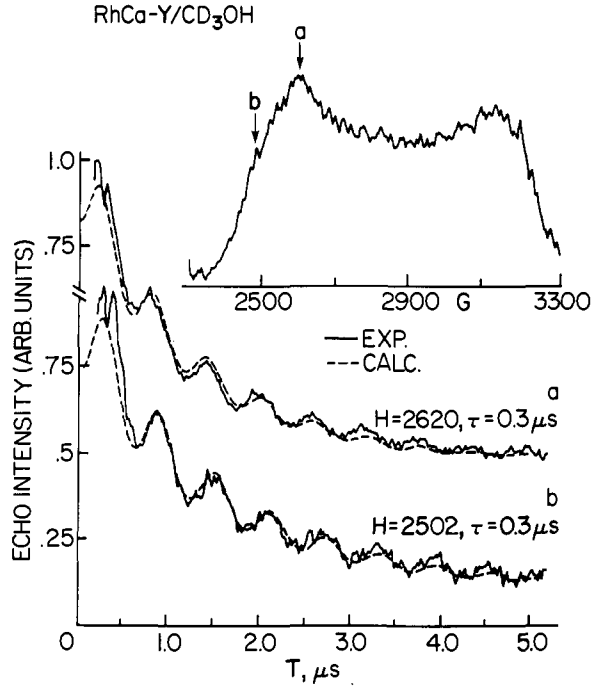

Figure 9. Field swept ESE of 1 wt % RhCa-Y activated at 400 °C after adsorption of CD_3OH recorded with $\tau = 0.40$ μs and ESEM recorded at field positions a and b. The ESEM at (a) is simulated with $A = 0.0$ MHz, $R = 0.46$ nm, and $N = 6$ and that at (b) simulated with $A = 0.0$ MHz, $R = 0.49$ nm, and $N = 9$.

spectra of samples activated to 400 °C and 500 °C (Figure 8, b and c).

Unlike RhNa-Y, modulation was observed from RhCa-Y after CD_3OH adsrption. The ESEM recorded at $H = 2500$ and 2620 G along with the field swept ESE are shown in Figure 9. Both ESEM correspond to 6 or 9 deuterons (2 or 3 methanol molecules) interacting at a relatively long distance of 0.46 or 0.49 nm, respectively. The same ESEM data were observed in RhNa-X[1] and RhCa-X.[3]

Adsorption of ammonia (ND_3) on both 1 wt % RhNa-Y and RhCa-Y generates similar ESR spectra as shown in Figure 10. The increase in spin concentration is greater than after methanol adsorption. In RhNa-Y (Figure 10d), the spectrum indicates the existence of four species: $g_\perp = 2.770$, $g_\perp(2) = 2.594$, and $g_\perp(3) = 2.405$, and $g_\parallel = 1.940$ where the last two values were assigned to one species on the basis of a comparison between the spectra before and after exposure to oxygen. In RhCa-Y the line at 2.405 is shifted to 2.379 (Figure 10a). Species N1 with $g_{zz} = 2.100$,

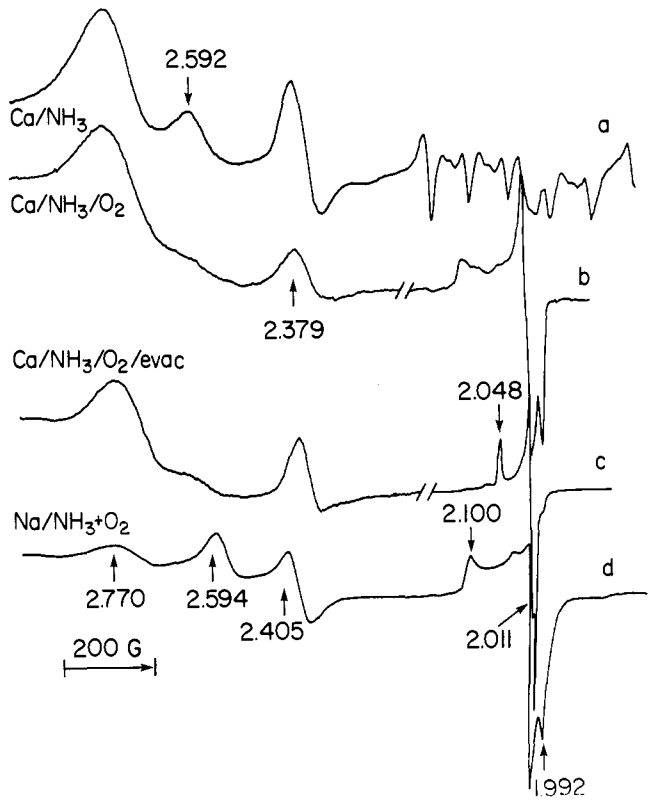

Figure 10. ESR spectra recorded at 77 K of (a) 1 wt % RhCa-Y activated at 500 °C after exposure to 70 Torr of ammonia, (b) same as case a after brief evacuation and exposure to 66 Torr of O_2 (the gain of the high field part is 8×10^2), (c) same as case b after brief evacuation (the gain of the high field part is 1.25×10^3), and (d) 1 wt % RhNa-Y after adsorption of 16 Torr of NH_3 in the presence of traces of oxygen. The gains unless otherwise stated are 1.6×10^3, 1.6×10^3, 1.6×10^3, and 6.3×10^2, respectively.

$g_{xx} = 2.011$, and $g_{yy} = 1.992$ is the fourth species. This species appears in the corresponding RhCa-X[3] sample through in considerably larger amounts. Exposure to O_2 causes broadening of the line at $g = 2.379$ and reduces the intensity of the line at $g = 2.594$ (Figure 10b) which is not restored after evacuation and reintroduction of ammonia at room temperature. The exposure to oxygen enhanced the N1 signal, whereas subsequent evacuation revealed the existence of an O_2^- species with $g_{zz} = 2.048$, $g_{yy} = 2.008$, and $g_{xx} = 2.003$ (Figure 10c). These values are very close to those of a O_2^- species generated in Ca-Y by γ-irradiation ($g_{zz} = 2.0458$, $g_{yy} = 2.008$, and $g_{xx} = 2.0017$).[23] In both cases the spectrum at room temperature is similar to the 77 K spectrum indicating no motion at room temperature.[23] When the sample was reexposed to ammonia the relative intensity of the O_2^- species decreased considerably. The nature of this species was discussed previously.[3] It is located in the α-cage and is either a Rh(II) cation directly coordinated to ammonia ligands where the unpaired electron is located on Rh(II) or a Rh complex with ammonia and O_2^- acting as a ligand where the unpaired electron is mostly on the oxygen. Adsorption of ammonia on RhNa-X generated mostly species C;[1] however, oxidation at 200 °C and subsequent ammonia adsorption generated spectra similar to those observed in RhNa-Y and RhCa-Y although the intensity is weaker.[2] Both the RhCa-Y and RhNa-Y samples gave no echo thus no further information concerning these species could be obtained.

Atanasova et al.[5] have observed similar ESR spectra in RhNa-Y with some differences. The spectrum could be observed only after prolonged exposure and heating to 130 °C. Both in RhCa-Y and in RhNa-Y the ESR signal appeared after 5–10

(23) Chamulitrat, W.; Kevan, L. *J. Phys. Chem.* **1985**, *89*, 4989.
(24) Van Brabant, H.; Schoonheydt, R. A.; Pelgimo, J. In *Metal Micro-Structures in Zeolites*; Jacobs, P. A. et al., Eds.; Elsevier: Amsterdam, 1982; pp 12–16.

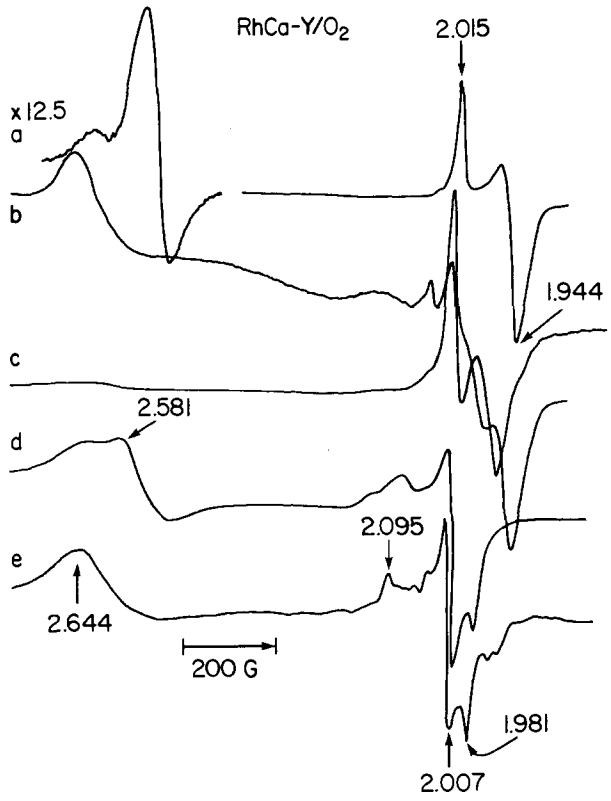

Figure 11. ESR spectra at 77 K of (a) 1 wt % RhCa–Y activated at 400 °C and exposed to 80 Torr of O_2, (b) 3 wt % RhCa–Y activated at 500 °C, oxidized at 200 °C, and evacuated at room temperature, (c) same as case b after exposure to 9 Torr of O_2, (d) 1 wt % RhCa–Y activated at 440 °C after simultaneous exposure to O_2 and D_2O, and (e) same as case d after simultaneous exposure to O_2 and methanol. The relative gains are 3.2×10^2, 8×10^2, 9×10^1, 2.8×10^2, and 8×10^2, respectively.

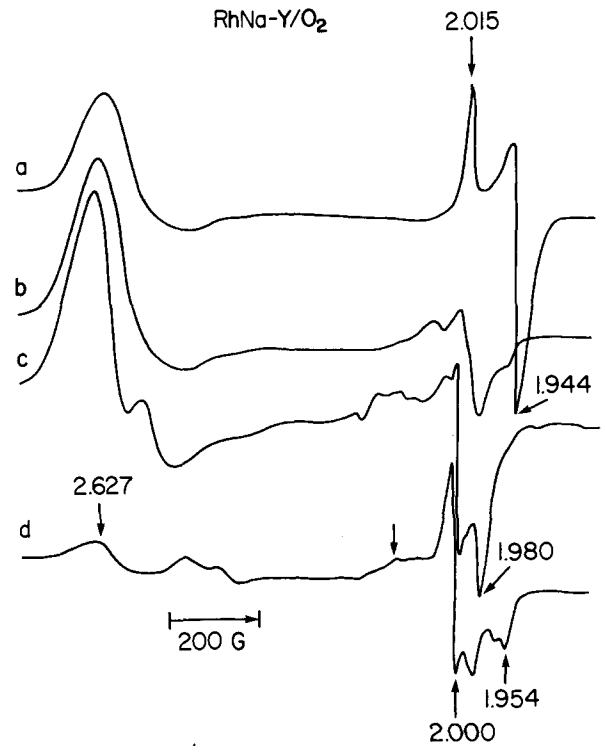

Figure 12. ESR spectra at 77 K of (a) 3 wt % RhNa–Y exposed to 10 Torr of O_2; (b) 3 wt % RhNa–Y activated at 500 °C, oxidized at 200 °C, and evacuated, (c) 1 wt % RhNa–Y activated at 500 °C after simultaneous adsorption of O_2 and D_2O, and (d) same as case c after simultaneous adsorption of O_2 and CD_3OH. The relative gains are 7.2×10^1, 2×10^2, 3.2×10^2, and 4×10^2, respectively.

min of exposure. Heating the RhNa–Y after ammonia adsorption to 300 °C for 3 h destroyed the ESR signal.

Adsorption of O_2 and CO. Both RhCa–Y and RhNa–Y activated at 400–500 °C gave an adduct with $g_\parallel = 2.015$ and $g_\perp = 1.944$ when exposed to oxygen at room temperature (Figures 11a and 12a). Similar adducts were previously reported for RhCa–X[3] and RhNa–Y.[4,5]

In RhCa–Y the signals corresponding to species C, A, and the O_2 adduct were not broadened by excess oxygen (80 Torr) whereas in RhCa–X species A is not observable when the oxygen pressure is 20 Torr and at 80 Torr the adduct signals show significant broadening. In RhNa–Y the increase from 1 wt % to 3 wt % Rh loading caused a linear increase in the adduct signal. Increasing the oxygen pressure to 32 Torr resulted in the appearance of additional lines overlapping with the adduct lines.

Oxidation with 200 Torr of O_2 at 200 °C and subsequent evacuation produces signals in the $\mathbf{g} = 2$ region (Figures 11b and 12b). The RhNa–Y signals are similar to those observed in RhNa–X after the same treatment. Exposure to 9 Torr of O_2 at room temperature restored the original adduct (Figure 11c) both in RhNa–Y and in RhCa–Y, suggesting that the adduct precursors were not affected by the oxidation. The signals appearing after O_2 adsorption are assigned to a Rh–oxygen adduct as also suggested in ref 4 and 5 and not to an O_2^- species on the basis of the $\mathbf{g}$ values.[3]

Adsorption of water and methanol in the presence of oxygen generated species near $\mathbf{g} \simeq 2$ in addition to the species obtained following adsorption of water or methanol alone (Figures 11d,e and 12c,d). We did not attempt ESE measurements on the O_2/methanol sample due to the relatively large number of species.

The ESR spectrum after water adsorption is simpler and similar to the one observed in RhCa–X.[3] In RhNa–Y (Figure 12c) it consists mostly of species C and another species with $g_{xx} = 2.007$, $g_{yy} = 1.981$, and $g_{zz} = 2.100$. Similar species have been reported in RhNa–Y and RhH–Y.[4,6] ESEM measurements reported by Narayana et al.[6] in RhH–Y suggested that the later species was coordinated to 4 deuteriums at 0.29 nm with $A = 0.1$ MHz. The ESEM pattern we observed is shown along with the field swept ESE in the upper part of Figure 13. Two sets of parameters gave reasonable fits: $A = 0.1$ MHz, $R = 0.32$ nm, and $N = 4$ and $A = 0.1$ MHz, $R = 0.30$ nm, and $N = 3$. The ambiguity between $N = 3$ and 4 is probably caused by neglecting the quadrupole tensor. The difference between our results and those of Narayana et al. could be due to the two-pulse interferences in the latter.[6]

The ESEM obtained from RhCa–Y along with the field swept ESE and the correspondance with the ESR spectrum are shown at the bottom of Figure 13. ESEM spectra were recorded at the two positions indicated by the arrows and both traces were best simulated with $A = 0.15$ MHz, $R = 0.3$ nm, and $N = 3$.

These species could be generated in RhNa–X by oxidizing the activated sample at 200 °C, evacuating at room temperature, and then adsorbing water or methanol.[2] In all cases[1,2] RhCa–X, RhCa–Y, RhNa–Y, and RhNa–X three major lines appeared at $\mathbf{g} = 2.10$, 2.007, and 1.981 and Naccache et al.[4] assigned them to a single species. However, different relative intensities in the various zeolites studied and shoulders appearing mainly on the $g_\parallel$ feature suggest the existence of several species with overlapping $\mathbf{g}$ tensors. These are discussed in ref 2 and 3.

In Table I are listed ESEM results obtained for the various Rh-exchanged zeolites exposed to O_2 and then water or methanol. The distribution in the distance is fairly small (0.29–0.33 nm), but the number of interacting deuterons varies from 2 to 4, which is wider than perhaps expected. N may vary in part due to neglecting the quadrupole interaction in the simulations, to several overlapping species which can have different contributions to the echo intensity in the various samples, and to differences in the ligands, i.e., OD groups vs. D_2O.

Adsorption of CO on RhCa–Y and RhNa–Y gives an Rh^{II}–CO adduct with $g_\perp = 2.173$ and $g_\parallel = 1.991$ (Figure 14). This signal disappeared upon evacuation. The same adduct was generated in RhCa–X[3] and was previously observed by Naccache et al. in RhNa–Y.[4] Adsorption of CO on 3 wt % RhNa–Y did not affect species C which was generated after activation (Figure 14a).

Table I. ESEM Data Obtained from the Various Rh-Exchange Zeolites after Exposure to Oxygen and Water or Methanol

zeolite	adsorbate	g value	A (MHz)	N	R (nm)	ref
RhCa-X	O_2/D_2O	2.00	0.1	3	0.32	3
	O_2/D_2O	1.98	or 0.1	3	0.33	
			0.1	2	0.29	
RhCa-X	O_2/CH_3OD	2.00	0.0	2	0.35	3
		1.98	0.1	2	0.30	
RhNa-X	O_2(200 °C)/D_2O	2.00	0.1	2	0.32	2
	O_2(200 °C)/D_2O	1.98	0.1	4	0.33	
RhNa-X	O_2(200 °C)/CD_3OH	2.00	0.0	6	0.47	2
RhCa-Y	O_2/D_2O	2.00	0.15	3	0.30	this work
		1.98	0.15	3	0.30	
RhNa-Y	O_2/D_2O	2.00	or 0.1	4	0.32	this work
			0.1	3	0.30	
RhNa-Y	O_2/D_2O	2.00	0.1	4	0.29	6

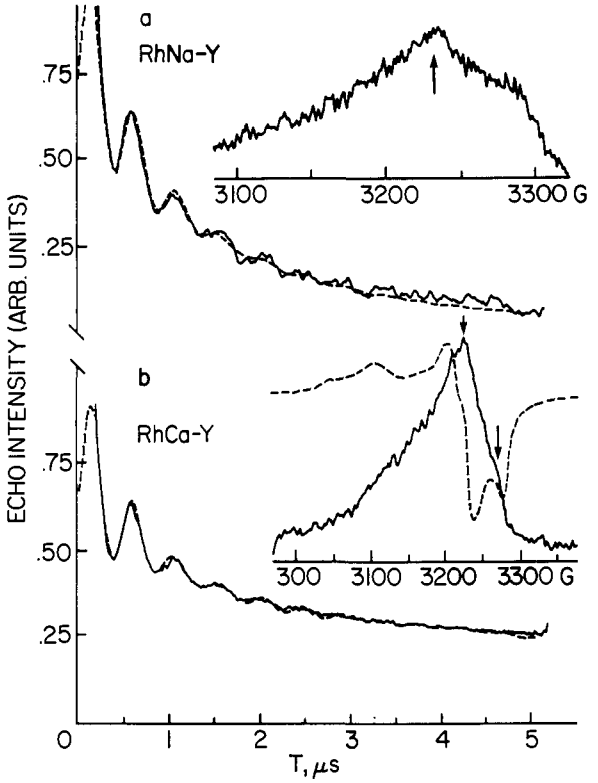

Figure 13. (a) Field swept ESE (τ = 0.30 μs) and the ESEM recorded at H = 3247 G and τ = 0.28 μs of 1 wt % RhNa-Y after simultaneous adsorption of O_2 and D_2O. The solid line represents the experimental data and the dashed line the best fit calculated ESEM with A = 0.1 MHz, R = 0.32 nm, and N = 4. (b) Same as case a for the corresponding RhCa-Y sample. The field swept ESE was obtained with τ = 0.32 μs; the ESR spectrum is also depicted as a dashed line. ESE experiments were performed at the positions indicated by the arrows. The experimental ESEM was recorded at H = 3286 G with τ = 0.29 μs. The calculated trace (- - -) was obtained with A = 0.15 MHz, R = 0.3 nm, and N = 3.

Adsorption of benzene on RhNa-Y activated at 400 °C did not change the ESR spectrum thus benzene does not induce dissociation of diamagnetic Rh dimers.

Discussion

Most of the paramagnetic Rh species which are generated in RhNa-Y and RhCa-Y have been previously observed in RhNa-X[1,2] and/or RhCa-X.[3] The various species have been identified and their formation has been previously discussed.[1-5] Accordingly, we will not repeat the detailed arguments for their identification and location in the zeolite structure but present the general methodology. The structure of X and Y zeolites along with the cation crystallographic sites are well-known from powder X-ray diffraction.[25] X and Y zeolites have three types of cages:

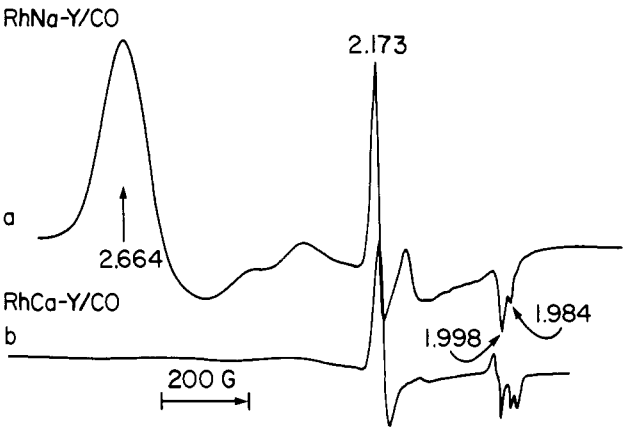

Figure 14. ESR spectra recorded at 77 K of (a) 3 wt % RhNa-Y activated at 380 °C after CO adsorption and (b) 1 wt % RhCa-Y activated at 500 °C after CO adsorption. The relative gains are 2 × 10^2 and 4 × 10^2, respectively.

(a) the hexagonal prism which is too small to accommodate adsorbed molecules but which can host one cation at site I, (b) the β-cage with a 0.22-nm access diameter which allows penetration of small molecules such as water and which contains cation sites I′ and II′, and (c) the α-cage which has an access of 0.74 nm. The α-cage has a variety of cation sites such as II, II*, III, and IV and can accommodate a rather large number of molecules. Analysis of the effects of adsorption on the ESR spectra and on the ESEM data in terms of distances between the Rh cation and the adsorbates in light of the zeolite structure, access opening, and adsorbate size leads to the determination of the location of the Rh species. For instance, the assignment of species C in RhNa-X[1] to site I in the hexagonal prism was based on large interaction distances of the Rh with CD_3OH, ND_3, and D_2O. Table II lists all the identified Rh(II) species formed after activation, reduction, oxidation, and adsorption of various adsorbates. In this section we discuss the RhCa-Y and RhNa-Y results in comparison with the RhNa-X[1,2] and RhCa-X[3] results to understand the effects of the cocations and the Si/Al rations on the formation of Rh(II) species in X and Y zeolites. In general, RhNa-Y, RhCa-Y, and RhCa-X show similar characteristics while RhNa-X shows different characteristics than the other zeolites.

After activation the same species, A and C, form in all four zeolites; they differ only in their relative concentrations. Species A, formed at activation temperatures of 320–400 °C, shows rather similar **g** values in all four zeolites, but in RhNa-X its relative amount seems higher and the $g_\perp$ feature shows a smaller splitting due to a somewhat less symmetrical environment. Species A is probably located in the sodalite cage in site II′ or in site II in the hexagonal windows facing the larger α-cage.[1] When the sample is activated to higher temperature in all zeolites and at all Rh loadings, species A vanishes and the spin concentration decreases.

The disappearance of species A may be explained as follows. In the temperature range 320–400 °C Rh(II) is still coordinated to a OH^- group formed from hydrolysis during the exchange

(25) Breck, D. W. In *Zeolite Molecular Sieves*; John Wiley & Sons: New York, 1974; pp 66–99.
(26) Goldfarb, D.; Kevan, L. *J. Phys. Chem.*, submitted for publication.

Table II. A Summary of the Major Rh(II) Species Formed in RhNa–X, RhCa–X, RhNa–Y, and RhCa–Y Zeolites with Suggested Site Locations in Parentheses

pretreatment/adsorbate	RhNa–X	RhNa–Y	RhCa–X	RhCa–Y
activation/400 °C	A (II or II′)	A (weak) (II or II′)	A (weak) (II or II′)	A (weak) (II or II′)
activation/500 °C	C (I)	C (I)	C (weak) (I)	C (weak) (I)
hydration	C (I)	I (β- or α-cages)	I (β- or α-cages)	I (β- or α-cages)
methanol	C (I)	C or I + H2 (β-cage)	C (weak) (I)	C (weak) (I)
ammonia	C (I)	C + N1 (weak) (I + α-cage)	N1 (α-cage)	N1 (weak) (α-cage)
O_2		Rh^{II}–O_2 (α-cage)	Rh^{II}–O_2 (α-cage)	Rh^{II}–O_2 (α-cage)
CO		Rh^{II}–CO (α-cage)	Rh^{II}–CO (α-cage)	Rh^{II}–CO (α-cage)
O_2/D_2O[a]	O1–O6 (I′ or II′)	O5, O4, O1 (II or II′)	O5, O4, O1 (II or II′)	O5, O4, O1 (II or II′)
O_2/methanol	O1–O6 (I′ or II′)	O5, O4, O1 (II or II′)	O5, O4, O1[b] (II or II′)	O5, O4, O1[b] (II or II′)
H_2[c]	H1 + H2 (α-cage + β-cage)	H2 (β-cage)		

[a] See ref 2 and 3. [b] And other species. [c] Heated to 150–200 °C.

procedure. As the temperature is increased above 400 °C dehydroxylation occurs. The "bare" Rh(II) at low loadings (1 wt %) can form Rh^{II}–Rh^{II} and/or Rh^{II}–O–Rh^{II} species which are both diamagnetic. The existence of rhodium oxide after activation in flowing oxygen has been previously reported.[24] These dimer species are located in either the α- or β-cages. Another possibility is that the Cl^- is still coordinated to the Rh(II) at 400 °C and at higher temperature it is removed as a Cl atom reducing the Rh(II) to Rh(I) or forming Rh^{II}–Rh^{II} and/or Rh^{II}–O–Rh^{II} by HCl abstraction. In this case using ESR and ESEM we could not tell whether Cl^- is still coordinated or not. Cl has a nuclear spin of $^3/_2$ and one might hope to see modulation effects if the chloride is not too close. However, due to a very short phase memory time of species A we could not observe an echo and could not check this possibility. Hyperfine splitting did not show in the ESR spectrum, although it may just be too small to be resolved.

Activation to 500 °C yields species C, located in site I in the hexagonal prism.[1,3] In RhCa–X and RhCa–Y (1–3 wt %) the relative concentration of species C after activation is small considering the total amount of Rh present because of the affinity of Ca^{2+} for site I.[25] In RhNa–X and RhNa–Y, as already mentioned, the amount of species C depends on the Rh loading. When the Rh-exchange level is ~6 cations per unit cell the species C signal is prominent and is about the same in RhNa–X and RhNa–Y. At this exchange level 12 Na^+ cations were removed. If some of these were removed from site I′, it would make site I more accessible. The Rh(II) can be stabilized at site I without the need to form dinuclear species in the larger cages.

Exposure to O_2, CO, and H_2 should not change much the distribution of the various charge balancing cations since these are not strong ligands and do not replace the framework oxygen ligands. Accordingly, the response of activated samples to these gases should provide information concerning the distribution of Rh cations following activation. In RhNa–X and RhNa–Y species A is more readily reduced then species C which is in good agreement with their suggested sites, i.e., II or II′ vs. I. All four zeolites showed the appearance of new signals following reduction which indicated the existence of remaining Rh(III) after activation. However, a unique H1 species located in the α-cage is only generated in RhNa–X.[1]

Reduction of RhNa–Y activated to 500 °C generated species H2 which was also generated in RhNa–X[2] and assigned to the β-cage. The same species is formed in RhNa–Y after absorption of methanol which indicated that the methanol molecule, which cannot enter the β-cage, reacted in the α-cage with either a Rh species or acidic sites to produce a small enough product, maybe hydrogen, which can enter the β-cage and reduce Rh(III) located there to Rh(II). This phenomenon was unique to RhNa–Y.

CO and O_2 are too large to enter the β-cage at room temperature, thus species interacting with them must be located in the α-cage or in site II. One major difference between RhNa–X and RhCa–X, RhCa–Y, or RhNa–Y is the formation of the O_2 and CO adducts in the latter three zeolites. The relative amounts of both of these adducts is RhCa–X $\simeq$ RhCa–Y > RhNa–Y. In RhNa–Y the relative amounts of species C and the O_2 and CO adduct in a 3 wt % sample is ~10:1.

The origin of the Rh^{II}–O_2 adduct formed in the α-cage is still not well understood. It could be formed by oxidation of two adjacent Rh^I to form $[Rh^{II}–O_2–Rh^{II}]^{2-}$ as suggested by Naccache et al.[4] or by interaction with Rh^{II}–Rh^{II} dimers to form Rh^{II}–O_2. The latter does not explain the relatively higher spin concentration after O_2 adsorption compared to hydration. If the precursor of the Rh^{II}–O_2 adduct is a Rh^I cation, the absence of that adduct in RhNa–X can be explained by the inaccessibility of Rh^I to O_2 which implies location in the β-cage which has an opening too small for oxygen penetration at room temperature. This is supported by the fact that oxidation at 200 °C of RhNa–X did produce ESR signals assigned to species in the β-cage.[2] If the dimers are the precursor of Rh^{II}–O_2 they are also located in the β-cage where the oxygen cannot induce dissociation of the dimer and displacement of the Rh cations. Why RhNa–Y behaves more like RhCa–X and RhCa–Y rather than like RhNa–X is not clear. It could be related to the number of cations since RhNa–X has almost twice as many cations.

The nonexistence of the CO adduct in RhNa–X is a further indication of the inaccessibility of the Rh(II) dimers in RhNa–X.

The Rh(II) species formed can be divided into two main groups. One group has $g_\perp > g_\parallel$ with a large anisotropy, broad lines, and $g_\perp$ in the range of 2.7–2.3. These species are usually formed after activation and after interaction with polar adsorbates such as water, methanol, and ammonia. The CO adduct is also included in the group although its $g_\perp$ is somewhat lower. These **g** values are indicative of a $d_{z^2-r^2}$ ground state and a tetragonally distorted octahedral symmetry.[1] The second group has **g** values in the range of 2.1–1.94 with $g_\parallel > g_\perp$. Their formation usually involves oxygen in one of the stages of preparation. For RhNa–X, formation involves oxidation at 200 °C, subsequent evacuation, and then adsorption. In the other three zeolites, formation involves exposure to O_2 at room temperature and subsequent adsorption of water, methanol, or ammonia. Group one species usually appear along with group two species, which supports the different origins of these two groups of species.

Although after activation the spin concentration differs from one zeolite to another, after hydration the signal intensities are rather similar. The major species in RhNa–X is C while in RhNa–Y, RhCa–X, and RhCa–Y it is species I which is directly

coordinated to water molecules. All four zeolites show additional similar species which are easily removed after evacuation at room temperature. These species could not be characterized due to overlapping ESR signals with species C or I signals. The relative intensity of these species seems to depend both on the cocation present and on the Si/Al ratio.

With adsorbates other than water, the number of Rh(II) species formed in RhNa–X[1] is less compared to the other zeolites and species C seems to be the dominant species after interaction with most adsorbates. This is probably due to the inaccessibility of the Rh(II) monomers and dimers to the various adsorbates which cannot enter the β-cage except for water. In RhNa–Y, RhCa–Y, and RhCa–X, unlike RhNa–X, the paramagnetic Rh species either form dimers or other Rh(II) species in the α-cage which renders them available to interact with the various adsorbates. RhCa–Y and RhNa–Y generate a greater number of paramagnetic species than RhCa–X after adsorption of ammonia, methanol, or O_2/methanol.

The inaccessibility of the Rh species in RhNa–X is also demonstrated by ethylene adsorption. In RhNa–X the adsorption of ethylene does not induce any changes in the ESR signal,[1] whereas in RhCa–X a new ESR signal appears which decays over a period of 15 min, indicating the involvement of Rh(II) in a reaction with ethylene.[26]

It is not clear why the adduct precursors are not generated in the α-cage in RhNa–X. It may be due to crowding of the α-cage with Na^+ cocations which does not permit precursor formation there. Thus Rh(II) monomer and dimers are formed in the hexagonal prism and β-cage, respectively. It is also possible that the accessibility of site I in RhNa–X to Rh species stabilizes Rh(II) so that it does not form dimers in the larger cages.

Overall, it seems that the accessibility of the Rh(II) species to adsorbates depends on a lesser number of cocations being present which is a function of both the Si/Al ratio and the cocation charge. With a higher Si/Al ratio, as in Y zeolite, the number of cations decreases and with a larger cocation charge, as for divalent cations, the number of cations decreases. This generalization accounts for why RhNa–X behaves differently from RhCa–X, RhNa–Y, or RhCa–Y.

Conclusions

The mechanism of dehydrogenation of Fe(2-octyne)$^+$ (Scheme V) could be distinguished recently by demonstrating that the product $(FeC_8H_{12})^+$ formed is best described as **34** not by Fe$(C_4H_6)_2^+$ complexes like **31**.[21]

Exchanging Na^+ in RhNa–Y with Ca^{2+} does not seem to have a great effect on the Rh(II) species generated. The only significant differences are the following: (1) the relative concentration of species C is higher in 3 wt % RhNa–Y than in 3 wt % RhCa–Y, and (2) species H2 appears after adsorption of methanol in RhNa–Y. The exchange of Na^+ by Ca^{2+} in X zeolite as well as the increase in the Si/Al ratio from RhNa–X to RhNa–Y shows a significant affect on the accessibility of the Rh(II) species. The increase of the Si/Al ratio from RhCa–X to RhCa–Y does not show any significant changes besides the appearance of some additional species in RhCa–Y after ammonia adsorption. When the number of cations is rather large, as in the case of RhNa–X, reducing the number either by exchange with a divalent cation or by increasing the Si/Al ratio affects the formation of paramagnetic Rh species. However, when this number is not large so that the zeolite cages are less crowded with cocations, as in RhNa–Y or RhCa–X, the above change has little effect.

Acknowledgment. This research was supported by the National Science Foundation and the Robert A. Welch Foundation. Essential equipment support was obtained from the Texas Advanced Technology Research Program and the Energy Laboratory of the University of Houston. D.G. thanks the Chaim Weizmann Foundation for a fellowship.

Vibrational Circular Dichroism of Optically Active Cyclopropanes. 3. *trans*-2-Phenylcyclopropanecarboxylic Acid Derivatives and Related Compounds

Sritana C. Yasui and Timothy A. Keiderling*

Contribution from the Department of Chemistry, University of Illinois at Chicago, Chicago, Illinois 60680. *Received August 13, 1986*

Abstract: Vibrational circular dichroism (VCD) data are presented for a series of (1*R*,2*R*)-*trans*-2-phenyl-1-(R-substituted)cyclopropanes where R = $COOCH_3$, $COOCD_3$, COOH, $CONH_2$, COCl, C≡N, CH_2OH, CD_2OD, CH_3, CD_3, and NH_2 (1*S*,2*R*). In addition, VCD for (1*S*,2*S*)-1-phenylpropylene oxide is presented for comparison. These data can be correlated to show certain characteristic, structure-indicating transitions common to all of the molecules. This is particularly true in the cyclopropane C–H stretching bands in the near-IR and less so of CH_2 deformations and ring modes in the mid-IR. To elucidate these comparisons it is necessary to interpret the frequency shifts of the characteristic bands as the substituent is varied. The range of compounds studied permits such an analysis for certain characteristic modes. The results for monocarbonyl and -cyano substitution further explain the presence and absence, respectively, of coupled oscillator VCD in the corresponding symmetrically disubstituted cyclopropyl compounds.

Vibrational circular dichroism (VCD) is a relatively new spectroscopic technique having demonstrated high sensitivity to conformational variation among molecules of similar structure.[1,2] Utilization of VCD for conformational analyses is just beginning to be explored. Two approaches can be followed to achieve this goal: one can correlate spectra of a series of related compounds in order to determine characteristic VCD bands, such as the topic of this paper, or one can attempt to calculate VCD by using one of the many theoretical models now available.[1-3] The latter approach demands previous evaluation of the usefulness of the calculational model with molecules of known structure. To this end, we have sought to obtain VCD of small, conformationally limited molecules on which a variety of theoretical approaches might be attempted.[4]

(1) Keiderling, T. A. *Appl. Spectr. Rev.* **1981**, *17*, 189.

(2) Nafie, L. A. In *Advances in Infrared and Raman Spectroscopy*; Clark, R. J. H., Hester, R. E., Eds.; Heydon: London, 1984; Vol 11, pp 49–93. Nafie, L. A. In *Vibrational Spectra and Structure*; Durig, T. R., Ed.; Elsevier: New York, 1981; Vol 10, pp 153–225. Nafie, L. A.; Diem, M. *Acc. Chem. Res.* **1979**, *12*, 296.

(3) Polavarapu, P. L. In *Vibrational Spectra and Structure*; Durig, J. R., Ed.; Elsevier: New York, 1984; Vol 13, pp 103–160.

0002-7863/87/1509-2311$01.50/0